

RSC Advances



This is an *Accepted Manuscript*, which has been through the Royal Society of Chemistry peer review process and has been accepted for publication.

Accepted Manuscripts are published online shortly after acceptance, before technical editing, formatting and proof reading. Using this free service, authors can make their results available to the community, in citable form, before we publish the edited article. This *Accepted Manuscript* will be replaced by the edited, formatted and paginated article as soon as this is available.

You can find more information about *Accepted Manuscripts* in the [Information for Authors](#).

Please note that technical editing may introduce minor changes to the text and/or graphics, which may alter content. The journal's standard [Terms & Conditions](#) and the [Ethical guidelines](#) still apply. In no event shall the Royal Society of Chemistry be held responsible for any errors or omissions in this *Accepted Manuscript* or any consequences arising from the use of any information it contains.

Microwave-assisted Synthesis of La-Cr co-doped SrTiO₃ and Their Photocatalytic Hydrogen Evolution under Visible Light

Fanpeng Cai,^a Yadong Meng,^b Bo Hu,^b Yubing Tang,^a Weidong Shi,^{b}*

^a School of Biology and Chemical Engineering, Jiangsu University of Science and Technology, Zhenjiang, 212003, P. R. China.

^b School of Chemistry and Chemical Engineering, Jiangsu University, Zhenjiang, 212013, P. R. China.

Abstract:

The increasing need for efficient materials capable of solar fuel generation is primary to the development of a green energy economy. In this contribution, we demonstrate that La-Cr co-doped SrTiO₃ (STO) nano-particles obtained through a one-pot microwave-assisted method exhibit well visible light absorption. We finetune the content of the cation substitution in the structure of STO to develop high-efficiency visible-light-driven water splitting photocatalysts considering the discrete of the impurity levels created by dopants. In our study, drawing conclusion from experiment that photocatalytic hydrogen production performance was optimum when doping mol amount of La-Cr was 5%. The rational expression for high-performance photocatalysts of La-Cr co-doped STO materials are described.

Keywords: solar fuel generation, microwave-assisted method, hydrogen production, La-Cr co-doped SrTiO₃

1 Introduction

Hydrogen production by solar-driven photocatalytic water splitting on the surface of semiconductors is a promising strategy to transform solar energy into hydrogen fuel¹⁻⁷. Sunlight driven water splitting is considered to be viable to produce hydrogen energy on account of water and sunlight are naturally abundant on the earth. Since the photocatalytic splitting of water into H₂ and O₂ on the surface of semiconductor was first reported, much attention had been paid to semiconductor materials which could be used as photocatalyst⁸⁻¹². In all the semiconductors, STO has been regarded as one of the most promising photocatalysts for water splitting because of its strong catalytic activity, high chemical and photochemical stability^{13,14}. However, STO shows activities only under ultraviolet irradiation accounting for merely about 4% of the incoming solar energy, which limits its practical application¹⁵. To overcome this defect, numerous studies have focused on extending the photocatalytic activity of STO toward the visible-light region.

Among them, doping of transition metals is a good strategy to develop visible light responsive photocatalysts if a suitable dopant is chosen¹⁶⁻¹⁹. The replacement of cations in the crystal lattice of STO may create impurity energy levels within the band gap of the photocatalyst that facilitate absorption in the visible range. However, it was reported that the impurity levels created by dopants in the photocatalysts are usually discrete, which would appear disadvantageous for the migration of the photogenerated holes²⁰. Therefore, we have reason to believe that it is important to finetune both the content and depth of the cation substitution in the structure of STO to develop visible-light-driven water-splitting photocatalysts. Although there has been extensive research on doped STO photocatalysts²¹⁻²⁶, little attention has been paid to the effects of the doped content of La and Cr.

In recent years, microwave-assisted synthesis has been developed to be a facile synthetic method for inorganic nano-scale materials in consideration of its shorter reaction time and higher reaction rate as compared to the conventional heating methods²⁷⁻²⁹. As a result, microwave heating has opened the possibility of realizing fast chemical reactions and rapid materials preparation in very short time periods,

usually in minutes, instead of hours or even days usually required by the conventional heating methods, leading to relatively low cost, energy saving, and high efficiency for materials production. On the other hand, the shorter crystallization time often leads to the small particle size of the product, which is essential for the synthesis of inorganic nano-scale materials. Thus, microwave-assisted synthesis is a promising synthetic method to obtain inorganic nano-scale materials.

There are some reports on La-Cr co-doped STO in the previous research, such as Ye et al. reported the reaction environment plays a significant role in the surface properties and thus affects the photocatalytic efficiency of La-Cr co-doped STO³⁰. However, the hydrothermal method in their work consumed 72 hours to prepare the sample, which neither efficient nor saving time. Up to date, there wasn't research on finetune the content of the La-Cr substitution in the structure of STO to develop efficient visible-light-driven water-splitting photocatalysts. What is more, we for the first time synthesize La-Cr co-doped STO by using a microwave-assisted method that is able to heat target materials without heating the entire furnace or oil bath, which saves time and energy. In this manuscript, La-Cr co-doped STO was prepared by a microwave-assisted method successfully. In our work, we fine tune the content of La-Cr cation substitution in the structure of STO to develop efficient visible-light-driven water splitting photocatalysts. As compared, La doped STO and Cr doped STO were prepared by the same method, respectively. The photocatalytic activities of the as-obtained La-Cr co-doped STO samples were evaluated in a Lab-H₂ photocatalytic hydrogen production system.

2 Experimental section

2. 1. Synthesis of La-Cr co-doped SrTiO₃ nano-particles

La-Cr co-doped SrTiO₃ nanoparticles was prepared by a facile microwave-assisted method. In a typical synthesis procedure, Sr(OH)₂·8H₂O (3.5mmol), TiO₂ (3.5mmol) and KOH (0.0375mol) were dissolved in 35 mL purified water. After stirred for about 30 min, a certain amount of La(NO₃)₃·6H₂O and Cr(NO₃)₃·9H₂O were dispersed into the solution under vigorous string. Then the as-obtained mixture was transferred into a Teflon-lined autoclave of 50.0 mL capacity.

The obtained mixture was heated in the microwave reactor (MDS-6, Shanghai Sineo Microwave Chemistry Technology Co., Ltd.) with the operating power of 800 W and working temperature of 150 °C for 5 h. After the container cooled into room temperature, the product was washed with deionized water by repeated centrifugation, and the productions were dried at 60 °C in air. Pure STO nanoparticles were prepared by the same method without an extra reagent of $\text{La}(\text{NO}_3)_3 \cdot 6\text{H}_2\text{O}$ and $\text{Cr}(\text{NO}_3)_3 \cdot 9\text{H}_2\text{O}$ introduced in the STO precursors liquid. Obtained samples with (La-Cr) /Sr mole ratio of 0, 1%, 2%, 4%, 5%, 6% and 8% was labeled as sample pure STO, La-Cr-1, La-Cr-2, La-Cr-4, La-Cr-5, La-Cr-6 and La-Cr-8. As compared, obtained samples with La/Sr and Cr/Sr mole ratio of 5% named as La-5 and Cr-5, respectively.

2.2. Characterization

Powder X-ray diffraction (XRD) patterns were obtained on a D/MAX-2500 diffractometer (Rigaku, Japan) using a $\text{Cu K}\alpha$ radiation source ($\lambda = 1.54056 \text{ \AA}$) at a scan rate of 7° min^{-1} to determine the crystal phase of obtained samples. Uv-vis absorption spectra of samples were measured by using UV-vis spectrometer (Shinadzu UV-2500). X-ray photoelectron spectroscopy (XPS) data were obtained by an ESCALa-b220i-XL electron spectrometer (VGScientific, England) using 300 W $\text{Al K}\alpha$ radiation. Transmission electron microscopy (TEM), high-resolution transmission electron microscopy (HRTEM) and HAADF-STEM mapping analyses were collected on an F20 S-TWIN electron microscope (Tecnai G2, FEI Co.), using a 200 kV accelerating voltage. The photoluminescence spectra was taken on a F4500 (Hitachi, Japan) photoluminescence detector.

2.4. Photocatalytic hydrogen production

The photocatalytic hydrogen production experiments were carried out in a Lab- H_2 photocatalytic hydrogen production system³¹. A 300W Xenon arc lamp was used as a light source and was positioned 20 cm away from the reactor in the system. In a typical water splitting over doped STO experiment, 100 mg of the prepared doped STO photocatalyst was dispersed with constant stirring in 200 mL of 20 vol% methanol aqueous solution. Prior to irradiation, the system was vacuumized to remove the dissolved oxygen. During the whole reaction process, vigorous agitation was

performed to ensure the uniform irradiation of the photocatalysts suspension. A certain amount of $\text{H}_2\text{PtCl}_6 \cdot 6\text{H}_2\text{O}$ aqueous solution was dripped into the system to load 0.5 wt% Pt into the surface of the photocatalyst by a photochemical reduction deposition method. The generated gas was collected intermittently through the septum, and hydrogen content was analyzed by the gas chromatograph (GC-SP7800, Beijing Jing Ke Ruida, China, TCD, nitrogen as a carrier gas and 5 Å molecular sieve column). All glassware was rigorously cleaned and carefully rinsed with distilled water prior to use.

3 Result and discussion

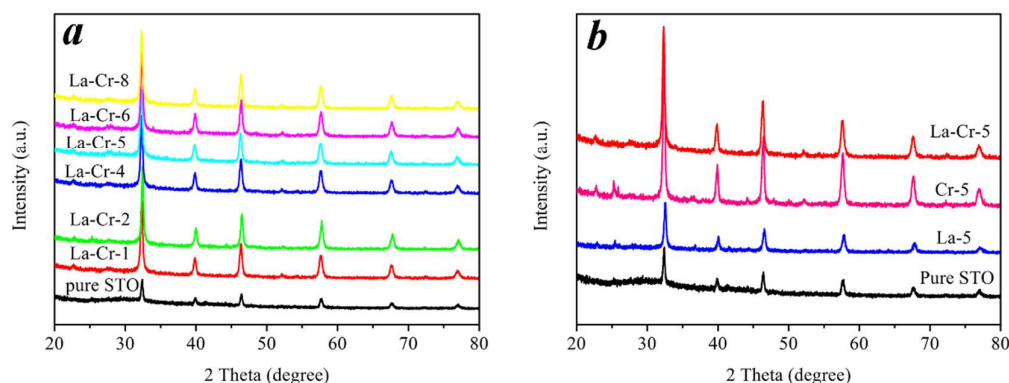


Fig. 1. (a) XRD patterns of pure STO and different La-Cr doping amount samples. (b) XRD patterns of La-Cr-5, Cr-5, La-5 and pure STO.

The crystal structures of the materials were investigated with powder X-ray diffraction (Figure 1). The XRD experiment confirms that all samples are pure single phase. Fig.1 shows the XRD patterns of pure STO and doped STO powder samples at room temperature, which reveal that both the pure and doped materials possess a homogeneous crystal structure of cubic perovskite symmetry (JCPDS card no. 05-0634). In our work, the La and Cr substitute the Sr and Ti, respectively (Q-JACS), and the radius of Cr and La is 0.615 Å and 1.032 Å, while the radius of Ti and Sr is 0.605 Å and 1.180 Å, respectively^{25,30}. Obviously, the radius of Ti is similar with Cr, and the radius of Sr is similar with La. As a result, the peak positions of the La-STO, Cr-STO and La-Cr-STO sample are almost the identical crystal structure as that of

STO (Fig. 1a and 1b), which also indicating that doping with La, Cr and La-Cr co-doping did not introduce any possible impurities.

The products in our manuscript are a cubic phase, and the lattice constant “a” of pure STO, Cr-5 and La-Cr-5 are 3.908, 3.911 and 3.910, respectively. As we can see, the lattice constant “a” of pure Cr-5 is bigger than that of pure STO, this is because the radius of Cr is 0.615 Å, which is bigger than that of Ti (0.605 Å). As a result, it is reasonable after Cr replace Sr. on the other hand, the radius of La is 1.032 Å, which is smaller than that of Sr (1.180 Å), which makes the lattice constant “a” of pure La-Cr-5 is shorter than that of Cr-5, and larger than that of pure STO.

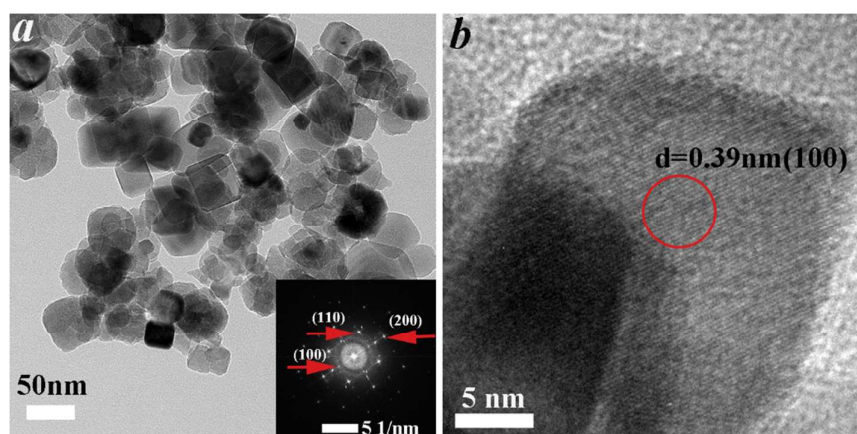


Fig. 2. TEM images, SAED patterns and HRTEM images of La-Cr-5 sample. (a) TEM image of La-Cr-5 sample, the insert is SAED pattern of La-Cr-5 sample. (b) HRTEM image of La-Cr-5 sample.

Fig. 2 displays the typical transmission electron microscopy (TEM) and high-resolution TEM (HRTEM) images of La-Cr-5 sample. As shown in Fig. 2a, it can be clearly observed that a great amount of the sample was dispersed as cubic particles with the average diameters of 60 nm for La-Cr-5. As shown in the SAED patterns (insert in Fig. 2a) taken from the nanoparticles in Fig. 2a revealed that La-Cr-5 nanoparticles had a single-crystalline structure. Furthermore, the SAED pattern shows a cubic array of sharp spots, and can be indexed as cubic phase, which is consistent with the XRD and TEM results. From the HRTEM image in Fig. 2b, the

lattice fringes can be clearly observed, suggesting the well-defined crystal structure, and the fringe with lattice spacing of ca. 0.39 nm corresponds to the (100) plane of the cubic STO. Furthermore, HRTEM images provide further evidence for the cubic structure of the La-Cr-5.

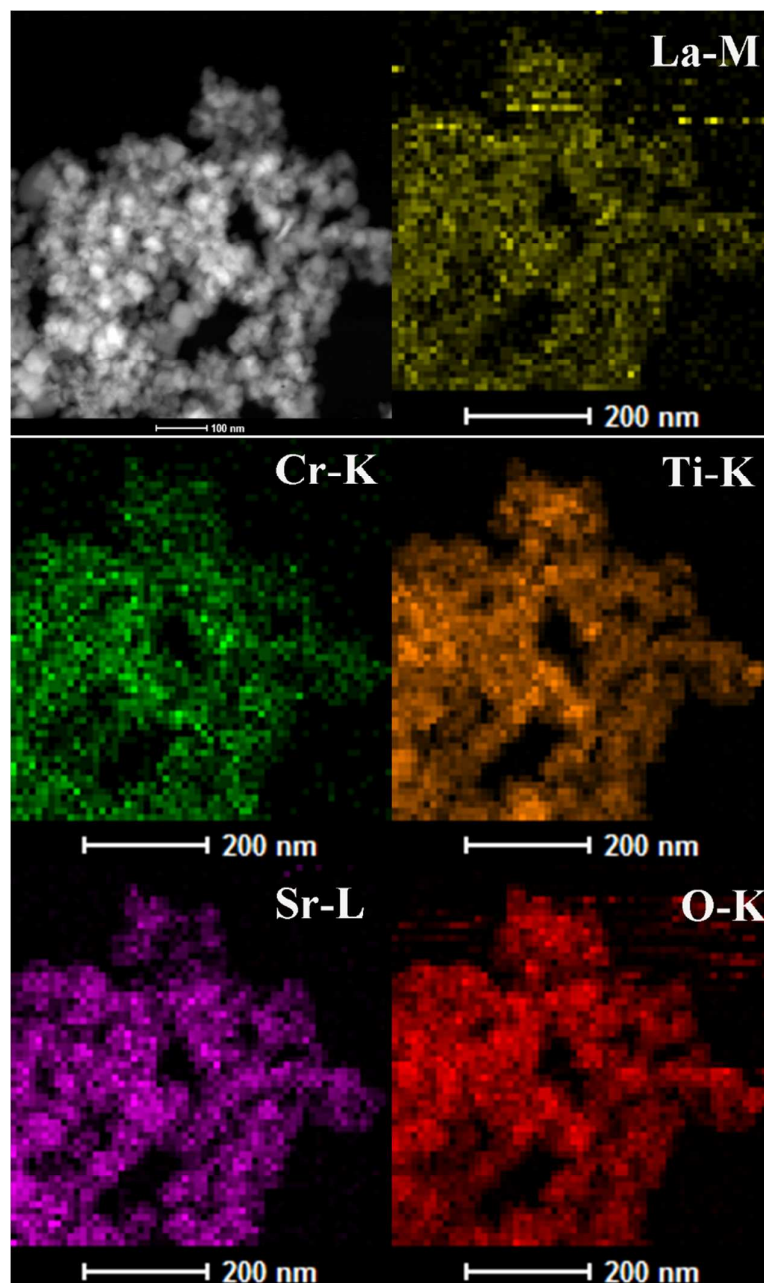


Fig. 3. Element mapping of La-M, Cr-K, Ti-K, Sr-L and O-K of La-Cr-5.

The structure of the La-Cr-STO inner space is further characterized by the scanning transmission electron microscopy (STEM), a very powerful characterization

instrument for determining the elemental distribution in material. As can be seen in Fig. 3, all of those signals for La (yellow), Cr (green), Sr (purple), O (red), and Ti (orange) are very uniform in the observation area, indicating the homogeneous distribution of Sr, O, Ti, La, and Cr in the composite. The above phenomena indicate that the successful co-doped of La-Cr into the STO crystal lattice and further confirm the formation of the La-Cr-Sr-Ti-O chemical bond during the present microwave-assisted hydrothermal process. By the way, the doping amount of Cr-5 and La-Cr-5 have been determined by the EDS and the result shown in Fig S1 and Fig S2.

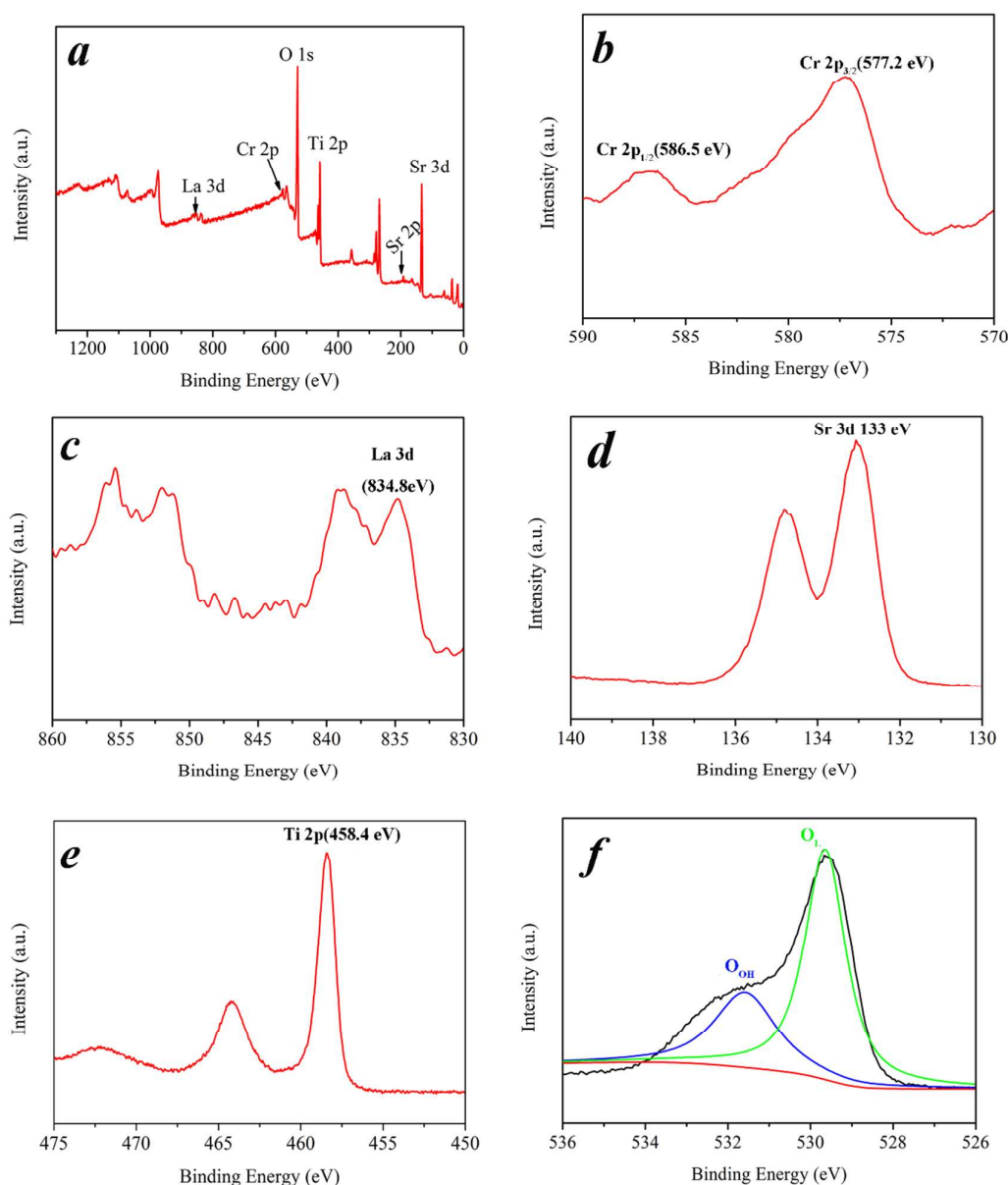


Fig. 4. (a) The full range XPS spectrum. (b) The high-resolution XPS spectrum of Cr 2p, (c) La 3d, (d) Sr 3d, (e) Ti 2p and (f) O 1s of La-Cr-2 sample, the different atomic species present at the surface are indicated as O_L = La-Cr-STO lattice oxygen and O_{OH} = oxygen from OH species.

As shown in Fig. 4b, the core level spectrum of the Cr 2p region shows two main peaks for Cr 2p_{1/2} and Cr 2p_{3/2} centered at ca. 586.1 eV and 577.2 eV, respectively, which are close to literature values and assigned to the Cr³⁺ state³². Experiments on the La-doped sample reveal the La core level 3d peaks depicted in Fig. 4c. The peaks are situated at 834.8eV which correspond to La³⁺ state³³. As shown in Fig. 4d, the binding energies of the Sr 3d with binding energies of ca. 133 eV which corresponding to that of the Sr²⁺. The XPS of the Ti (Fig. 4e) exhibited two different signals of Ti 2p_{3/2} and Ti 2p_{1/2} and 464.2 eV, respectively³⁴. The different atomic species present at the surface are indicated as O_L = TiO₂ lattice oxygen and O_{OH} = oxygen from OH species. The O 1s peaks of the present samples show a regular pattern (Fig. 4f) and show two components, corresponding to oxygen in the oxide lattice (O_L with binding energies of ca. 529.5eV), and to surface hydroxyl (O_{OH} with binding energies of ca. 531.7eV), and the peaks at 531.7 and 529.5 eV are ascribed to O 1s of H₂O and doped SrTiO₃, respectively³⁵⁻³⁹.

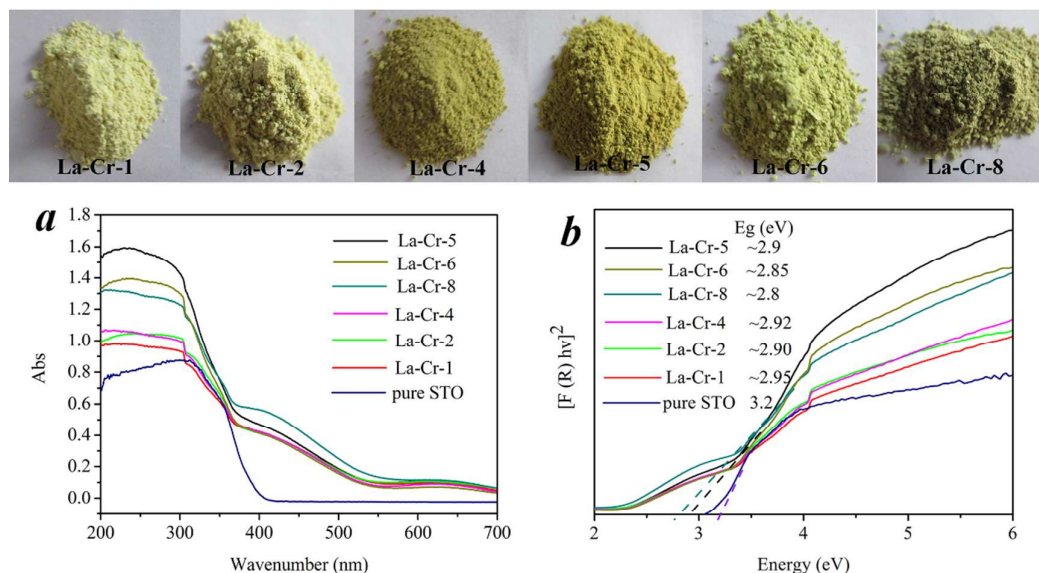


Fig. 5. (a) UV-vis absorption spectra of all doped samples, (b) Optical band gaps. The picture inset shows the color of all samples.

Introducing impurity levels or bands into the band gap of UV-active oxide semiconductors by incorporation of transition metals is considered to be an effective method of sensitizing the materials to visible light region for photocatalytic water splitting. As shown in Fig. 5a, the optical absorption of La-Cr co-doped STO exhibit a strong enhancement in the visible-light and ultraviolet region. Furthermore, the UV-vis absorption spectra of these doping materials suggested that the optical absorption properties increased with the increment of doping amount. Band gaps were calculated according to ultraviolet-visible absorption spectra as displayed in Fig. 5b, all doping materials showed narrower band gaps (~ 2.80 eV) than that of pure STO (3.20 eV). The shrinks in band gaps of the doped materials, which shift the valence band to a more negative position and may thus facilitate hydrogen evolution, are due to optical absorption properties increment. The picture insert in Fig. 5 shows the color of samples changes with the doped amount. Obviously, all samples exhibit yellow color, and increased doped amount accompanies with deeper color. The location of VB top-edge more negative, the oxidation potential will become worsened and worsened accompanying the performance of water splitting in methanol solution became low. And this reasoning would be verified in the experiments of photocatalytic hydrogen production in the next.

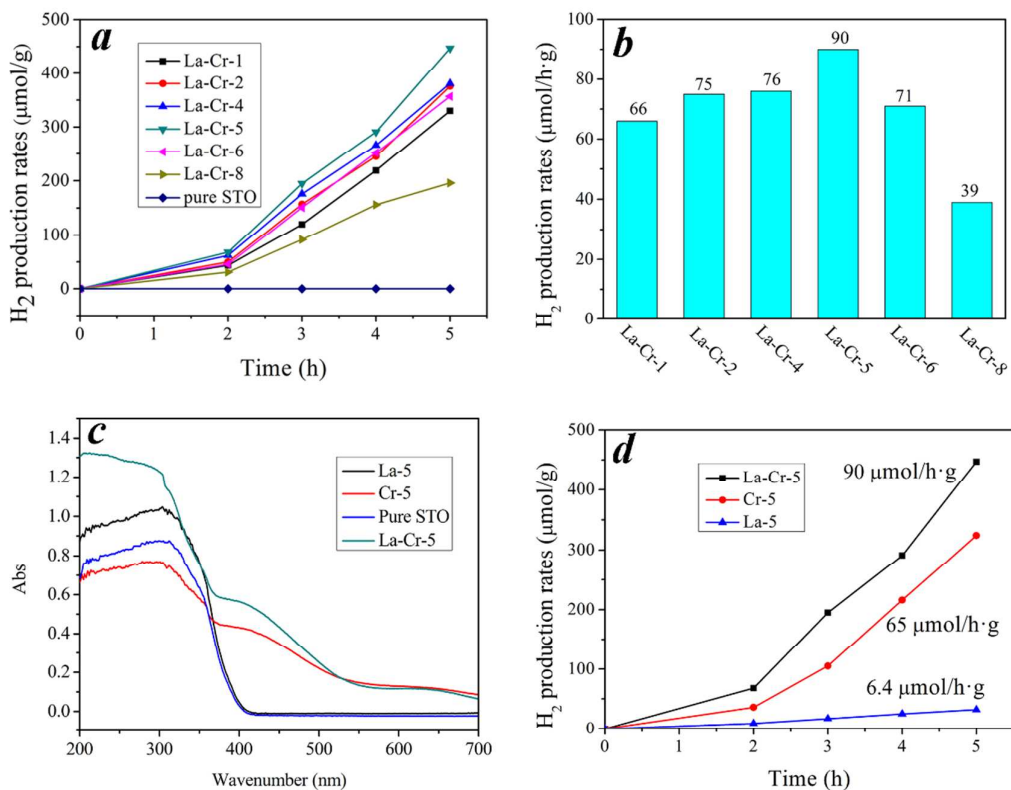


Fig. 6. (a) Typical reaction time course of the photocatalytic H₂ evolution of different doped amount STO materials under visible light irradiation. (b) Rates of H₂ evolution over doped STO. (c) UV-vis absorption spectra of La-Cr-5, La-5, Cr-5 and pure STO. (d) Comparison of the visible-light photocatalytic activity of samples La-Cr-5, La-5 and Cr-5 for the H₂ production. Reaction conditions: catalyst, 0.1 g; cocatalyst, Pt (0.5 wt%); reactant solution, 200 mL of 20 vol% aqueous methanol solution; light source, 300 W Xe lamp ($\lambda > 420$ nm).

Photocatalytic H₂ evolution experiment was carried out with the doped STO photocatalyst (loaded 0.5 wt % Pt cocatalyst) suspended in the CH₃OH solution. Figure 6a shows the typical reaction time course of the photocatalytic H₂ evolution of different doping amount materials. Obviously, doped STO shows excellent photocatalytic H₂ evolution performance under visible-light irradiation, but the pure STO has no activity. Increase of the La-Cr doping amount resulted in a progressive increase of the photocatalytic hydrogen evolution rate under visible-light irradiation, however, additional increase of the La-Cr content to 6 % (Fig. 6b) resulted in a decrease of the photocatalytic hydrogen evolution rate. It can be seen that La-Cr-5 showed the best ability for photocatalytic H₂ production, and the photocatalytic H₂

production rate is about 90 $\mu\text{mol/g}\cdot\text{h}$ as shows in Fig. 6b. Therefore, a suitable content of La-Cr is crucial for optimizing the photocatalytic activity of La-Cr-STO photocatalysts.

Fig. 6c shows the UV-vis absorption spectra of La-Cr-5, La-5, Cr-5 and pure STO. By comparison, UV-vis absorption data can accurately reveal what element doping to have been affected by the responding of optical absorption region. In details, Cr doped STO shows a strong enhancement of optical absorption in the visible-light region being accompanied by a weakening of light absorption in the ultraviolet region. La doped STO exhibits weak enhancement of optical absorption both in the visible-light and ultraviolet region. As for La-Cr co-doping STO, both a strong enhancement in the visible-light and ultraviolet region was observed. Therefore, we can conclude that the doped transition metal ions play an important role for the absorption bands observed in the visible light region for STO co-doped with La and transition metal Cr. As shown in Fig. 6d, the comparison of the visible-light photocatalytic activity of samples La-Cr-5, La-5 and Cr-5 for the H_2 production. Obviously, the La-Cr-5 possess the best photocatalytic activity, the photocatalytic hydrogen production rate of La-5 is very low, and that of Cr-5 is much higher than that of La-5 but is still lower than that of La-Cr-5. The improvement of activity of La-Cr-STO could be attributed to fewer defects and lower recombination rate of electrons and holes. The expression of this phenomena will be discussed in the next photoluminescence spectra.

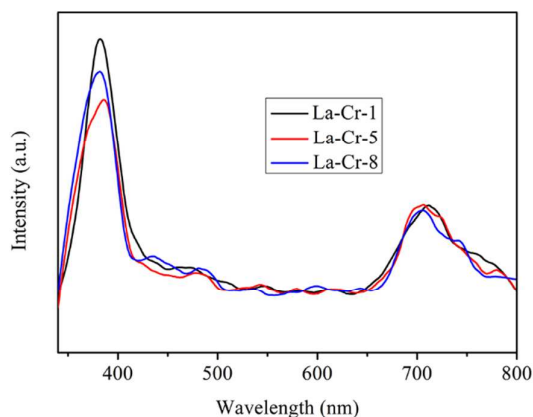


Fig. 7. The photoluminescence spectra of all samples (10 mg were well dispersed into 5 mL of ethanol) with excitation wavelength of 320 nm.

As can be seen in Fig. 5a, in comparison with La-Cr-1, La-Cr-5 and La-Cr-8, the intensity of the PL signal for La-Cr-5 is much lower. This indicates that the La-Cr-5 has a lower recombination rate of electrons and holes under visible-light irradiation, which is may due to the fact that the impurity levels created by dopants in the photocatalysts are usually discrete, when the doping amount is too high would appear disadvantageous for the migration of the photogenerated holes. Owing to the fewer defects in La-Cr-5, and the over potential is larger, which also results in best separation of charge and consequently causes best migration of charger carriers to active sites. The trend of the proton concentration and the trend of polymerization for the sample set are in very good agreement with the corresponding activity, which contributes to charge transport. By comparison, the photoluminescence spectra of Cr-5 and Cr-La-5 are shown in Fig S3, the discussion also provide in the ESI.

4 Conclusions

In summary, La-Cr co-doped STO was prepared by the microwave-assisted method successfully for the first time. The advantages of this approach are low cost, energy saving, and high efficiency. In this work, we fine tune the content of La-Cr cation substitution in the structure of STO to develop efficient visible-light-driven water splitting photocatalysts. The photoactivity is improved upon the La-Cr/Sr mole ratio changing from 1% to 5%, and decreased when the La-Cr/Sr mole ratio changing from 5% to 8%. In this paper, we give the scientific explanation between doping amounts and photocatalytic activity.

ACKNOWLEDGMENT

We gratefully acknowledge the financial support of the National Natural Science Foundation of China (21407067, 21276116, 21477050, 21301076 and 21303074), Excellent Youth Foundation of Jiangsu Nature Scientific Committee (BK20140011), Program for high-level innovative and entrepreneurial talents in Jiangsu Province,

Program for New Century Excellent Talents in University (NCET-13-0835), Henry Fok Education Foundation (141068) and Six Talents Peak Project in Jiangsu Province (XCL-025).

REFERENCES

1. K. Iwashina, A. Iwase, Y. H. Ng, R. Amal and A. Kudo, *Journal of the American Chemical Society*, 2015, 137, 604-607.
2. Q. Li, B. Guo, J. Yu, J. Ran, B. Zhang, H. Yan and J. R. Gong, *Journal of the American Chemical Society*, 2011, 133, 10878-10884.
3. D. J. Martin, P. J. Reardon, S. J. Moniz and J. Tang, *Journal of the American Chemical Society*, 2014, 136, 12568-12571.
4. X. Wang, S. Blechert and M. Antonietti, *ACS Catalysis*, 2012, 2, 1596-1606.
5. X. Wang, K. Maeda, A. Thomas, K. Takanabe, G. Xin, J. M. Carlsson, K. Domen and M. Antonietti, *Nature materials*, 2009, 8, 76-80.
6. Q. Xiang, J. Yu and M. Jaroniec, *Journal of the American Chemical Society*, 2012, 134, 6575-6578.
7. C. Xu, W. Yang, Q. Guo, D. Dai, M. Chen and X. Yang, *Journal of the American Chemical Society*, 2013, 135, 10206-10209.
8. B. Pant, H. R. Pant, N. A. M. Barakat, M. Park, T.-H. Han, B. H. Lim and H.-Y. Kim, *Ceramics International*, 2014, 40, 1553-1559.
9. M. Yang, S. Hu, F. Li, Z. Fan, F. Wang, D. Liu and J. Gui, *Ceramics International*, 2014, 40, 11963-11969.
10. T. Zhou, Y. Xu, H. Xu, H. Wang, Z. Da, S. Huang, H. Ji and H. Li, *Ceramics International*, 2014, 40, 9293-9301.
11. A. Kudo and Y. Miseki, *Chemical Society reviews*, 2009, 38, 253-278.
12. R. M. Navarro Yerga, M. C. Alvarez Galvan, F. del Valle, J. A. Villoria de la Mano and J. L. Fierro, *ChemSusChem*, 2009, 2, 471-485.
13. Q. Kuang and S. Yang, *ACS applied materials & interfaces*, 2013, 5, 3683-3690.
14. Y. Sasaki, A. Iwase, H. Kato and A. Kudo, *Journal of Catalysis*, 2008, 259, 133-137.
15. Y. Liu, L. Xie, Y. Li, R. Yang, J. Qu, Y. Li and X. Li, *Journal of Power Sources*, 2008, 183, 701-707.
16. K. Iwashina and A. Kudo, *Journal of the American Chemical Society*, 2011, 133, 13272-13275.
17. J. Xu, Y. Wei, Y. Huang, J. Wang, X. Zheng, Z. Sun, L. Fan and J. Wu, *Ceramics International*, 2014, 40, 10583-10591.
18. F. Yi, H. Li, H. Chen, R. Zhao and X. Jiang, *Ceramics International*, 2013, 39, 347-352.
19. F. Zou, Z. Jiang, X. Qin, Y. Zhao, L. Jiang, J. Zhi, T. Xiao and P. P. Edwards, *Chemical communications*, 2012, 48, 8514-8516.
20. G. J. D. a. P. H. M. d. K. G. Blasse, *Mat. Res. Bull.*, 1981, 16, 991-998.
21. T. Ishii, H. Kato and A. Kudo, *Journal of Photochemistry and Photobiology A: Chemistry*, 2004, 163, 181-186.
22. W. Wei, Y. Dai, M. Guo, L. Yu and B. Huang, *The Journal of Physical Chemistry C*, 2009, 113,

- 15046-15050.
23. Y. Jia, S. Shen, D. Wang, X. Wang, J. Shi, F. Zhang, H. Han and C. Li, *Journal of Materials Chemistry A*, 2013, 1, 7905.
 24. S. Shen, Y. Jia, F. Fan, Z. Feng and C. Li, *Chinese Journal of Catalysis*, 2013, 34, 2036-2040.
 25. J. Wang, T. Fang, S. Yan, Z. Li, T. Yu and Z. Zou, *Computational Materials Science*, 2013, 79, 87-94.
 26. P. Reunchan, S. Ouyang, N. Umezawa, H. Xu, Y. Zhang and J. Ye, *Journal of Materials Chemistry A*, 2013, 1, 4221.
 27. J. Sungpanich, T. Thongtem and S. Thongtem, *Ceramics International*, 2012, 38, 1051-1055.
 28. M. B. Suwarnkar, R. S. Dhabbe, A. N. Kadam and K. M. Garadkar, *Ceramics International*, 2014, 40, 5489-5496.
 29. Y. J. Zhu and F. Chen, *Chemical reviews*, 2014, 114, 6462-6555.
 30. S. Ouyang, H. Tong, N. Umezawa, J. Cao, P. Li, Y. Bi, Y. Zhang and J. Ye, *Journal of the American Chemical Society*, 2012, 134, 1974-1977.
 31. F. Cai, Y. Tang, H. Shen, C. Wang, A. Ren, L. Xiao, W. Gu and W. Shi, *CrystEngComm*, 2015, 17, 1086-1091.
 32. H. Kato and A. Kudo, *The Journal of Physical Chemistry B*, 2002, 106, 5029-5034.
 33. M. S. J. Marshall, D. T. Newell, D. J. Payne, R. G. Egdell and M. R. Castell, *Physical Review B*, 2011, 83.
 34. R. E. Tanner, Y. Liang and E. I. Altman, *Surface Science*, 2002, 506, 251-271.
 35. S. Ardizzone, C. L. Bianchi, G. Cappelletti, S. Gialanella, C. Pirola and V. Ragaini, *Journal of Physical Chemistry C*, 2007, 111, 13222-13231.
 36. G. Cappelletti, S. Ardizzone, C. L. Bianchi, S. Gialanella, A. Naldoni, C. Pirola and V. Ragaini, *Nanoscale research letters*, 2008, 4, 97-105.
 37. J. Chen, S. Shen, P. Guo, M. Wang, P. Wu, X. Wang and L. Guo, *Applied Catalysis B: Environmental*, 2014, 152-153, 335-341.
 38. K. Li, B. Chai, T. Peng, J. Mao and L. Zan, *ACS Catalysis*, 2013, 3, 170-177.
 39. Z. Li, P. Zhang, T. Shao, J. Wang, L. Jin and X. Li, *Journal of hazardous materials*, 2013, 260, 40-46.